

Advanced Curved Planar Reformation: Flattening of Vascular Structures

Armin Kanitsar*

Rainer Wegenkittl‡

Dominik Fleischmann†

Meister Eduard Gröller*

* Institute of Computer Graphics and Algorithms
Vienna University of Technology

† Department of Radiology
Stanford University

‡ TIANI Medgraph
Austria

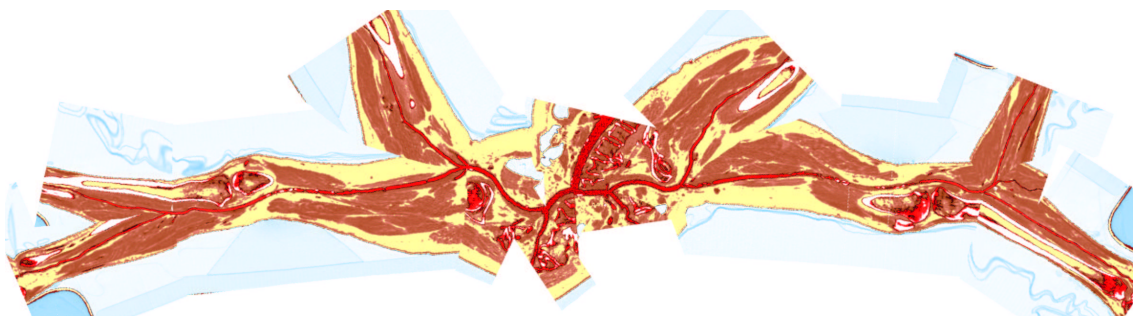


Figure 1: An untangled vascular tree of the peripheral arteries.

ABSTRACT

Traditional volume visualization techniques may provide incomplete clinical information needed for many applications in medical visualization. Especially in the area of vascular visualization important features such as the patent lumen of a diseased vessel segment may not be visible. Curved Planar Reformation (CPR) has proven to be an acceptable practical solution. Existing CPR techniques, however, still have diagnostically relevant limitations. In this paper we introduce two advanced methods for efficient vessel visualization, based on the concept of CPR. Both methods benefit from relaxation of spatial coherence in favor of improved feature perception. We present a new technique to visualize the interior of a vessel in a single image. A vessel is re-sampled along a spiral around the vessel central axis. The helical spiral depicts the vessel volume. Furthermore, a method to display an entire vascular tree without mutually occluding vessels is presented. Minimal rotations around the branching points of a vessel tree eliminate occlusions. For each viewing direction the entire vessel structure is visible.

CR Categories: J.3.2 [Computer Applications]: Life and Medical Sciences—Medical Information Systems I.3.3 [Computing Methodologies]: Computer Graphics—Picture/Image Generation

Keywords: computed tomography angiography, vessel analysis, curved planar reformation

1 INTRODUCTION

Non-invasive imaging of the vascular system with computed tomography (CT) and magnetic resonance imaging (MRI) has be-

come a well established alternative to invasive intraarterial angiography. CT and MRI provide high-resolution volumetric data sets of the human body. These data, however, may contain many objects of less or no diagnostic interest. This makes volume-rendering (i.e., Maximum Intensity Projection (MIP), ray casting, shaded surface display) without preprocessing often impossible or inaccurate.

CPR - Curved Planar Reformation is a way to visualize vascular structures with small diameter. High level information as the vessel's centerline is used to re-sample and visualize the data. The whole length of the tubular structure is displayed within a single image by this technique. Vascular abnormalities (i.e., stenoses, occlusions, aneurysms and vessel wall calcifications) are then investigated by physicians.

Current CPR techniques allow the investigation of the vessel lumen in a longitudinal section through the central axis of the vessel. However, vascular abnormalities might not be touched by this plane and therefore they do not appear in the generated image. One way to overcome this problem is to rotate the re-sampled plane around the central axis. This results in a set of images to be interpreted by the radiologist. A more comprehensive display of the entire vascular lumen in one representative image is highly desirable. A new visualization method was developed to overcome this limitation.

Another important aspect in computed *tomography angiography* (CTA) is the efficient visualization of treelike vascular structures using CPR display techniques. Multi-path CPR techniques based on a projective combination of vessel segments provide a spatially coherent display of the vascular anatomy [6]. However, parts of the arteries might be superimposed by other arteries depending on the intersecting plane. For a detailed inspection of the entire vascular tree different sections through the vessel's central axis have to be re-sampled. In order to have diagnostically valuable results the vessel lumen should be visible within each image. Thus a new technique for unobscured displaying of an arterial tree is proposed.

Section 2 describes related work in this area. In Section 3 a new method for visualizing the interior of a vascular structure is presented. A technique for displaying the entire vascular tree without overlapping arteries is presented in Section 4. Possible improvements and conclusions are discussed in Section 5.

*{kanitsar,meister}@cg.tuwien.ac.at, <http://www.cg.tuwien.ac.at/home/>

†dominik.fleischmann@univie.ac.at

‡{rainer.wegenkittl}@tiani.com <http://www.tiani.com/>

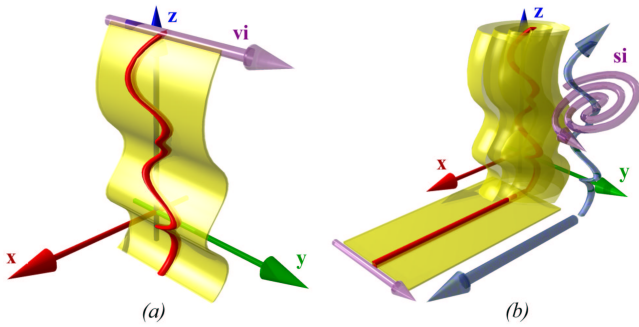


Figure 2: Traditional CPR (a), and helical CPR (b) generation.

2 RELATED WORK

The most important prerequisite for CPR visualization is an appropriate estimation of the vessel centerline. Latest CT technology, such as multiple detector-array CT, provide high resolution volumetric data sets. Due to the large size of these data sets (up to 1900 transverse cross-sectional images of the abdomen and entire legs), the manual definition of the vessel centerline is no longer an option. In this respect several algorithms [7, 10, 11] have been developed with different properties concerning reliability, speed and accuracy.

Avants and Williams presented a vessel tracking method consisting of two parts [2]. From user defined seed points a surface expansion is computed based on the eikonal partial differential equation. A minimal cost path is calculated from these regions. From this path a cross-sectional area/radius profile is generated.

He et al [5] proposed a path extraction method based on a two-dimensional region-growing algorithm with a subsequent shortest path algorithm. The resulting path was refined using the multi-scale medial response. The vascular tree is flattened in a semiautomatic method called *Medial Axis Reformation*.

Some authors propose to take the central-axis as an input for the generation of an abstract vessel-model. Abstract vessel-models allow fast rendering, as polygonal meshes of low complexity are generated [3]. Furthermore non-photorealistic rendering provides the possibility to emphasize global properties of the vascular tree [4].

Kanitsar et al [6] compared three methods for CPR generation: Projected CPR, stretched CPR and straightened CPR. In addition three extensions of CPR, developed to overcome the most relevant clinical limitations of CPR visualization have been proposed: Thick CPR, rotating CPR and multi-path CPR. The latter provides a display of a whole vascular tree within one image. While superimposition of bones and arteries is prevented, the intersection of arteries itself is not avoided.

Further information about the clinical relevance of the CPR visualization technique can be found in [9, 1, 8].

3 HELICAL CPR

The basic idea of helical CPR visualization is to display the interior of a vessel within one image. To accomplish this, a re-sampling strategy different from existing CPR methods is introduced. CPR techniques display re-sampled data in close vicinity of a surface intersecting the volume. This surface is defined by the central-axis of the vessel and a *vector-of-interest* (vi) (see Figure 2a). The latter might be defined in a local coordinate system of the central-axis. In any case the data are re-sampled in a linear way defined by the vector vi . The vector-of-interest describes the re-sampling direction which is orthogonal to the viewing direction.

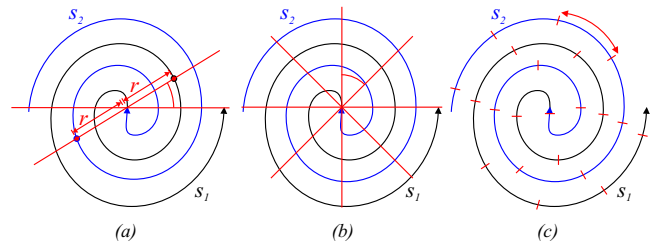


Figure 3: Spiral-of-interest (a), constant angle sampling (b), constant arc-length sampling (c)

The helical CPR method is based on a non-linear re-sampling of the data. The vector-of-interest as generating element for the surface is replaced by a *spiral-of-interest* (si) (see Figure 2b). This results in a convoluted surface around the central-axis. At a sufficiently small distance between each winding the vessel is intersected several times. Stenosis, calcification, and occlusions are included in the computed surface. This surface is helical and displayed.

3.1 Method Description

The helical CPR visualization technique is based on the straightened CPR method. Along the central-axis of the vessel cross-sections are calculated at an appropriate sampling distance. Within each section a local 2D coordinate system is defined. The center of the cross-section represents the estimated center of the vessel lumen from the corresponding center-line position. Starting from this center point two interleaved spirals s_1 and s_2 are computed (see Figure 3a). In order to maintain a uniform sampling of the vessel cross-sections a spiral with constant inter-winding distance was selected. This requirement is satisfied by the Archimedean spiral which can be notated in polar equation as:

$$r = a\theta \quad (1)$$

The transformation of points on the curve into Cartesian coordinates is straightforward. Thus the computation of each point X_{s_1} on s_1 and X_{s_2} on s_2 is performed as follows:

$$X_{s_1} = a\theta \begin{pmatrix} \cos \theta \\ \sin \theta \end{pmatrix} \quad X_{s_2} = a\theta \begin{pmatrix} \cos \theta' \\ \sin \theta' \end{pmatrix} \quad \text{where } \theta' = \theta + \pi \quad (2)$$

For an appropriate sampling of the vessel lumen the parameter a was set to $1/\pi$. This assures the constant distance between the windings of the two interleaved spirals to be one. The computed points X_{s_1} and X_{s_2} on the spiral are transformed back into volume space and re-sampled.

The center of each row in the final CPR image corresponds to the center of the vessel cross-section. Starting from this reference point the image space to the left is filled with data re-sampled by s_1 and to the right with data from s_2 .

3.2 Sampling Strategy

The current implementation of the helical CPR technique supports two sampling strategies for computing points from the spiral. The angle θ is increased by a constant angle ω for each point in the case of *constant angle* sampling (see Figure 3b). For each sampling step a constant distance Δ on the arc-length of the spiral is covered if *constant arc-length* sampling is applied (see Figure 3c).

Constant angle. For each point re-sampled from the spiral the generating angle θ is incremented by a fixed angle ω . Each winding is rendered into an equal sized area in the final image. Therefore the comparably densesampled area in close vicinity of the vessel center is amplified in image space. The resulting fish-eye zooming effect is achieved at the cost of increased distortion.

Constant arc-length. Given a fixed sampling distance Δ between two adjacent points on the spiral the increment ω of the angle θ is approximated. The increment ω is defined by the ratio of Δ and the circumference calculated from the most recent radius. As usually small sampling distances are used the error introduced by this approximation is negligible. The extent of the vessel in the CPR image is directly proportional to the area of the vessel lumen. Thus large vessels occupy a superproportional large image space.

3.3 Phantom Dataset

The images generated by helical CPR visualization provide a quite unconventional display of vascular structures. Therefore a phantom dataset containing a set of typical vascular abnormalities was computed. By means of this dataset the typical pattern of each anatomical case are demonstrated (see Figure 4).

The simulated vessel of the phantom dataset contains a semi-circumferential vessel wall calcification, and a circumferential vessel wall calcification without luminal stenosis. An eccentric "soft-plaque" stenosis and a segmental concentric high-grade stenosis was also simulated, respectively (top-down order). Figure 4a shows a direct volume rendering display of this simulated vessel. From this visualization method the flow channel within the circular vessel wall calcification can not be gauged. A coronal and sagittal straightened CPR is presented in Figure 4b and c. The partial vessel wall calcification as well as the eccentric stenosis are not visible in the sagittal straightened CPR. This demonstrates the need for different longitudinal sections. Figure 4d and e show the result of the helical CPR technique with constant arc-length and constant angle sampling. The vertical black lines indicate the image space required for one winding. Partial vessel abnormalities tend to reoccur in a separated fashion several times in the image whenever the area is intersected by a winding. Vessel pathologies clearly stand out in the helical CPR images. The helical CPR "peels-off" the bloodvessel. Thus the extent of abnormalities is enhanced.

3.4 Results

The application of an helical CPR technique on a real world dataset is presented in Figure 5. A constant angle and constant arc-length sampled helical CPR display is compared to a straightened CPR image. In contrast to the straightened CPR the helical CPR shows the area of vessel lumen instead of the diameter. The white arrow illustrates an example where the helical CPR outperforms a traditional CPR. The small flow-channel of the stenosis is not touched by the displayed longitudinal section of the straightened CPR and therefore not visible. However in both helical images this flow-channel is displayed. As eccentric lesions cause repetitive patterns in the image space, the attention of the observer is immediately drawn to those areas even if a lesion is not visible in a standard CPR display.

4 UNTANGLED CPR

The aim of untangled CPR visualization is to display a vascular tree without overlapping arteries independently from the spatial position of the intersecting plane. In order to accomplish this requirement the spatial relations of the projected vessels have to be relaxed. Branching points of the vessel tree are taken as pivot points.

Rotating the corresponding vessels around these pivot points in image space eliminates vessel overlaps. Keeping the introduced distortions small maintains fast perception and reduces the impact of re-sampling artifacts in the final image. Thus the applied transformations are restricted to the branching points (bifurcations) of the arterial tree. In addition to that this transformations should be appropriate in terms of changing the tree layout and appearance without violating the non-intersection criterion. The *non-intersection criterion* is defined in a way that two vessel hulls must not cross each other at any time. The definition of a vessel hull is described below.

The new CPR technique is based on the stretched CPR and multi-path CPR method introduced by Kanitsar et. al. [6]. This method maintains the curvature of the vessel to a high extent and preserves isometry. The vessel's curvature is crucial in approximating a geometrically undistorted appearance of the vessel tree. Isometry on the other hand is important for vascular investigations. Stent planning and stenosis grading estimation are possible in the final image.

The input of the algorithm is a tree graph representing the topology of the vascular structure. For each vessel segment the center line of the vessel is stored as a set of adjacent points at an appropriate sampling distance. In practice it turned out that diameter estimations of vessels are not reliable enough in certain cases. Therefore for the purpose of generality the algorithm does not take diameter information into account. However, the adaptation to this additional information would be straightforward.

4.1 Method outline

The untangling CPR method consists of four main steps. As all untangling calculations are performed in image space the tree graph is first mapped to image space using a stretched CPR projection. In a consecutive step the transformation of each subtree with respect to the non-intersection criterion is performed. Afterwards the image space is partitioned in a way that each vessel obtains those parts of the image space which are closest in scan-line direction. Finally the image is rendered.

Tree projection. The vascular tree is mapped to a projection plane coplanar to the viewing plane. For each two successive points the subsequent point is rotated around an axis defined by the previous point and the vector-of-interest. This rotation is carried out for each point starting from the root of the vascular tree. This produces a stretched vascular tree.

Untangling operation. From the projected tree graph in image space the necessary transformations for each node are calculated. This is done by recursively circumscribing the subtrees with vessel hulls. The first pass is bottom up maintaining only the correct transformation of the largest enclosing vessel hulls. In a second pass the final transformation for each vessel hull segment is accumulated top down.

Image space partitioning. Before rendering the final image the extent of each vessel segment is cropped in a way that no overlapping image areas remain. This process determines the starting point and the end point of each scan line for rendering.

Rendering. Each vessel strip is rendered separately. Conceptually the vessel strip is first extracted from the dataset using a stretched CPR mapping. Afterwards the strip is transformed to the position defined by the untangling process. In a further step the strip is clipped according to the space partitioning information. Finally each cropped scan line is rendered into the image.

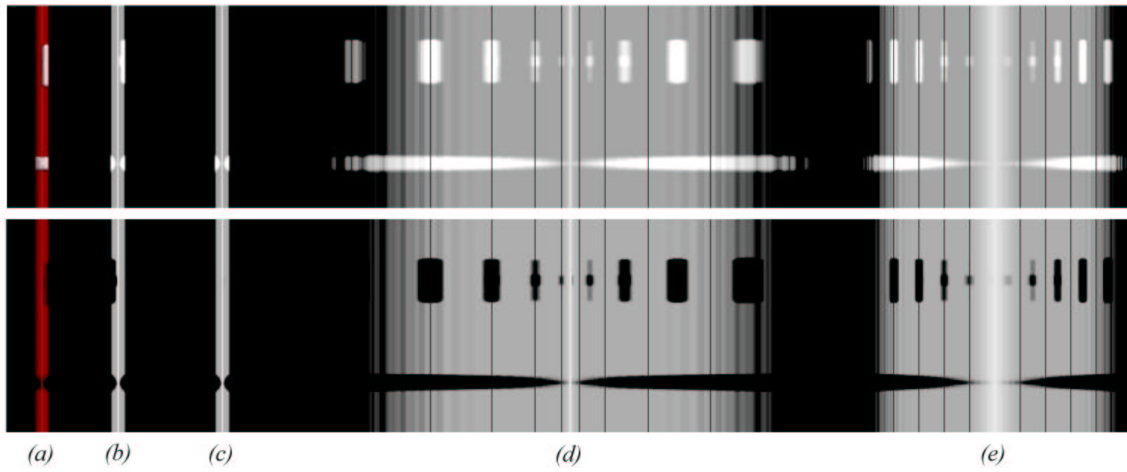


Figure 4: Phantom dataset: Direct volume rendering (a); Coronal (b) and sagittal (c) straightened CPR; Helical CPR with constant arc-length (d) and fixed angle (e).

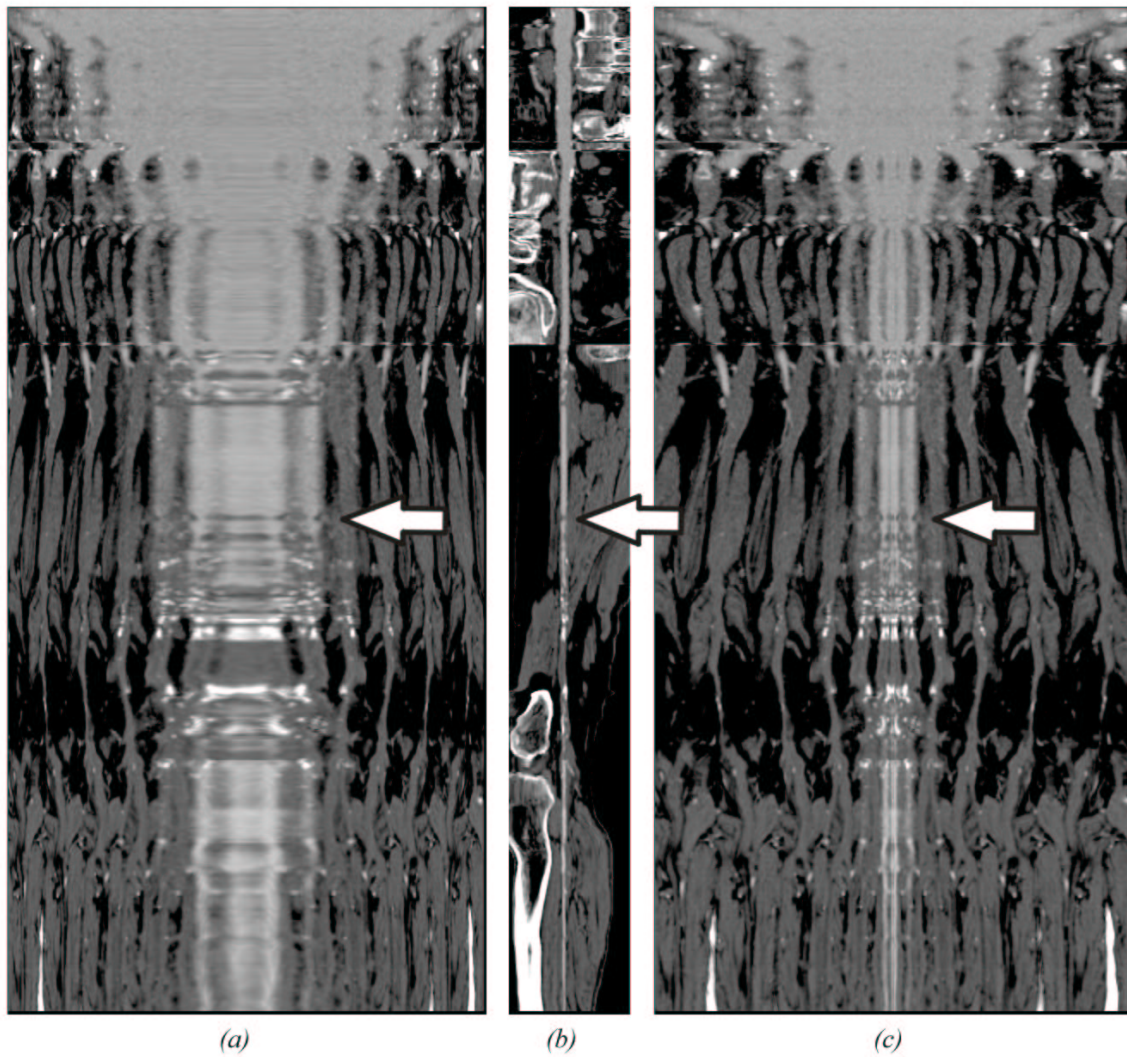


Figure 5: A straightened CPR (b), an helical CPR with constant angle sampling (a), and constant arc-length sampling (c) of a real world dataset.

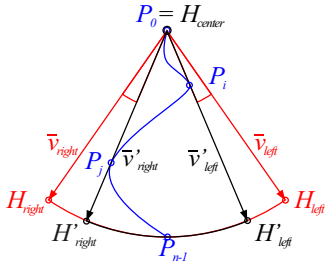


Figure 6: The vessel hull primitive

4.2 The vessel hull primitive

The *vessel hull* is the basic primitive for further intersection tests. It encloses the vessel's centerline in image space as shown in Figure 6. The centerline is given as a set of points $P = \{P_0, \dots, P_{n-1}\}$. A vessel hull is a sector of a circle. The root of a vascular subtree defines the center point H_{center} . A matrix $\mathfrak{R}_{H_{center}}$ associated with each center point describes a rotational transformation of the subsequent tree. The points H'_{right} and H'_{left} result from a conservative estimation of the leftmost and rightmost extent of the enclosing subtree seen from the center point.

The vessel hull encloses the centerline of the vessel thus two neighboring vessels touching each other is not prevented by this primitive. To overcome this situation the vessel hull is enlarged by a small angle ϵ as depicted in Figure 6. Depending on the size of the inspected vessels this ϵ may be adjusted by the user on the fly. However an $\epsilon \leq 2^\circ$ was found to be appropriate for most tested datasets. If the vessel diameter is known at the extremal points P_i and P_j then ϵ can be easily calculated more accurately. The points comprising the ϵ -tolerance are referred to as H_{right} and H_{left} .

Each vessel hull primitive can be described as a tuple of $V = \{H_{center}, H_{left}, H_{right}, \mathfrak{R}_{H_{center}}\}$ where $\vec{v}_{left} = \overrightarrow{H_{center}H_{left}}$ and $\vec{v}_{right} = \overrightarrow{H_{center}H_{right}}$.

4.3 Putting things together

A rule based approach is applied for combining vessel hulls from various parts of the vascular tree (see Figure 7). The projected vessel tree is approximated by an enclosing hierarchy of vessel hulls. This hierarchy is constructed bottom up. Combining two vessel hulls at a branching point involves a rotation around the common pivot point H_{center} . This results in a new larger hull which bounds the entire subtree. Constructing the vessel hull hierarchy involves several cases which are discussed in the following. A vessel hull created from the vessel centerline is based on *case 1*. Neighboring vessel hulls are combined according to *case 2*. An enclosing vessel hull from two consecutive vessel hulls is created in *case 3*. The assembling process is done bottom up. This results in a binary tree of vessel hulls where each node is represented by a vessel hull circumscribing all subjacent vessel hulls.

Case 1. The center point H_{center} is defined by the first point P_0 of the vessel segment. The first point on the convex hull of the vessel segment in clockwise orientation is denominated as point P_i and in counterclockwise direction as point P_j . Because of the stretched CPR mapping from volume to image space, point P_{n-1} is the point with maximum distance from P_0 . Thus the radius of the vessel hull is computed as $|P_{n-1} - P_0|$. The normalized vectors \vec{v}_{left} and \vec{v}_{right} represent the directions from H_{center} to P_i and P_j respectively. These vectors are scaled according to the radius of the vessel hull. The

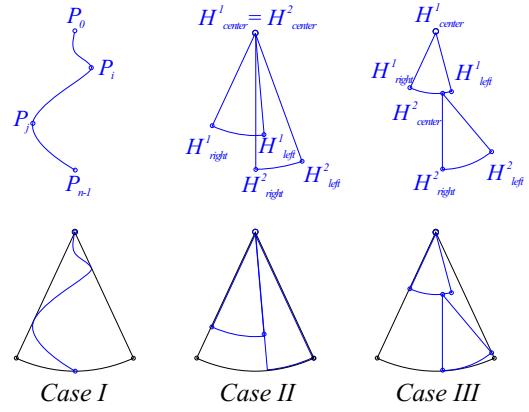


Figure 7: The three vessel hull combination cases.

tolerance angle ϵ is incorporated by a transformation with \mathfrak{R}_ϵ and $\mathfrak{R}_{-\epsilon}$. Finally H'_{right} and H'_{left} are computed.

Case 2. For the case of two adjacent vessel hull primitives (V^1 and V^2) (see Figure 7) the ordering of the subtrees has to be determined first. According to this decision the left vessel hull with respect to $H_{center} = H^1_{center} = H^2_{center}$ is denominated as V^l and the right one as V^r . If the vessel hull primitives overlap, an untangling angle γ is computed from \vec{v}'_{left} and \vec{v}'_{right} (see Figure 11a). From this angle the rotational matrices $\mathfrak{R}_{H^1_{center}}$ and $\mathfrak{R}_{H^1_{center}}$ are calculated. These matrices define a transformation of the vessel hull primitives V^r and V^l in a way that the primitives do not overlap anymore. This implies a transformation of the associated vascular subtree (see Figure 11a). If the vessel hull primitives do not overlap the matrices are simply the identity matrix.

The vectors \vec{v}_{left} and \vec{v}_{right} of the combined vessel hull are computed from the transformed vectors \vec{v}'_{left} and \vec{v}'_{right} . The radius of the enclosing vessel hull is defined by the maximum radius of V^1 and V^2 . From this information H_{left} and H_{right} is computed. The newly generated vessel hull encloses the non-overlapping underlying vessel hulls.

Case 3. The combination of two successive vessel hulls is straightforward. V^1 is considered to be the predecessor of V^2 as depicted in Figure 7. H^1_{center} is taken as the new center point H_{center} of the enclosing vessel hull. The direction to the rightmost point of H^1_{right} and H^2_{right} with respect to H_{center} is considered to be \vec{v}_{right} . Vector \vec{v}_{left} is calculated likewise. The radius of the new vessel hull V is defined by the maximum distance from H_{center} to H^1_{right} , H^1_{left} , H^2_{right} , and H^2_{left} .

Case 3 is similar to the 2nd case. However no additional transformation is introduced during this step. This is because undersampled areas occur under this circumstances as shown in Figure 11b.

Any treelike vascular structure can be processed using this set of rules. One bifurcation for instance is subdivided into three *case 1*, one *case 2* and, one *case 3*. The recursive algorithm finishes with a hierarchy of enclosing vessel hulls where the root hull contains the entire vessel tree. A detailed description of each assembling case in abstract notation is given in Figure 8.

Case 1:

$$\begin{aligned}
H_{center} &\leftarrow P_0 \\
\vec{v}_{right} &\leftarrow P_j - H_{center}, \{P_j | P_j, \ell \in P \wedge \forall \ell (\ell \text{ left of } \overrightarrow{H_{center}P_j})\} \\
\vec{v}_{left} &\leftarrow P_i - H_{center}, \{P_i | P_i, \ell \in P \wedge \forall \ell (\ell \text{ right of } \overrightarrow{H_{center}P_i})\} \\
rad &\leftarrow |P_{n-1} - P_0| \\
H_{right} &\leftarrow H_{center} + rad \cdot (\mathfrak{R}_e \star \vec{v}_{right} / |\vec{v}_{right}|) \\
H_{left} &\leftarrow H_{center} + rad \cdot (\mathfrak{R}_{-e} \star \vec{v}_{left} / |\vec{v}_{left}|)
\end{aligned}$$

Case 2:

$$\begin{aligned}
H_{center} &\leftarrow H_{center}^1 \\
(V^1, V^2) &\leftarrow \text{if (changeOrder) then } (V^2, V^1) \text{ else } (V^1, V^2) \\
\mathfrak{R}_{H_{center}^1} &\leftarrow \text{RotationMatrix}(H_{center}, -0.5 \max(\langle \vec{v}_{left}, \vec{v}_{right} \rangle, 0)) \\
\mathfrak{R}_{H_{center}^2} &\leftarrow \text{RotationMatrix}(H_{center}, +0.5 \max(\langle \vec{v}_{left}, \vec{v}_{right} \rangle, 0)) \\
\vec{v}_{right} &\leftarrow \vec{v}_{right} \\
\vec{v}_{left} &\leftarrow \vec{v}_{left} \\
rad &\leftarrow \max(rad^1, rad^2) \\
H_{right} &\leftarrow H_{center} + rad \cdot (\mathfrak{R}_{H_{right}} \star \vec{v}_{right} / |\vec{v}_{right}|) \\
H_{left} &\leftarrow H_{center} + rad \cdot (\mathfrak{R}_{H_{left}} \star \vec{v}_{left} / |\vec{v}_{left}|)
\end{aligned}$$

Case 3:

$$\begin{aligned}
H_{center} &\leftarrow H_{center}^1 \\
\vec{v}_{right} &\leftarrow \text{if } (H_{right}^2 \text{ left of } \overrightarrow{H_{center}H_{right}^1}) \text{ then } H_{right}^1 \text{ else } H_{right}^2 \\
\vec{v}_{left} &\leftarrow \text{if } (H_{left}^2 \text{ right of } \overrightarrow{H_{center}H_{left}^1}) \text{ then } H_{left}^1 \text{ else } H_{left}^2 \\
rad &\leftarrow \max(rad^1, |H_{center} - H_{right}^2|, |H_{center} - H_{left}^2|) \\
H_{right} &\leftarrow H_{center} + rad \cdot \vec{v}_{right} / |\vec{v}_{right}| \\
H_{left} &\leftarrow H_{center} + rad \cdot \vec{v}_{left} / |\vec{v}_{left}|
\end{aligned}$$

Figure 8: Assembling of vessel hulls.

4.4 Layout definition

The decision of the vessel hull ordering in *case 2* has a significant impact on the layout of the displayed vascular tree. Two different approaches have been investigated (see Figure 9). One possibility is a left-to-right ordering based on the spatial relations of the vascular tree according to the currently used viewing direction. In this case the ordering is based on the spatial location of the vessel hulls according to the current viewing direction. This approach is referred to as *adaptive layout*. In contrast to that a *fixed layout* was investigated too. The fixed layout is independent from the viewing direction. In the present prototype implementation the vessel ordering of the coronal display is maintained for all viewing directions. For clinical routine applications a standardized ordering might be a reasonable solution. According to this standardization the left-most artery for peripheral CTA examinations might be the left deep femoral artery (profunda femoris) followed by the left anterior tibial artery and so on.

The advantage of an adaptive tree layout is a more efficient utilization of image space and less distortion introduced by the untangling operation compared to a fixed layout. The introduced distortion measured by the sum of untangling angles γ over a 360° rotation of a peripheral CTA dataset is depicted in Figure 10. However, in the case of an adaptive tree layout discontinuities occur whenever the ordering of the vessels change. Thus the inspection of a sequence of images becomes more difficult as the identification of each vascular segment becomes more difficult. Labelling the vessel segments eases this limitation for examinations carried out on a set of images.

4.5 Image space partitioning

Bevor rendering the final image the image space has to be separated into fragments for each vascular structure. This step is necessary because arteries are possibly obscured by bones if multiple layers are rendered into a single image area (see [6] for details).

A principle drawing direction is associated with each vessel segment. Each point of the projected vessel center line maintains a *scan line* deduced from this principal drawing direction. These scan

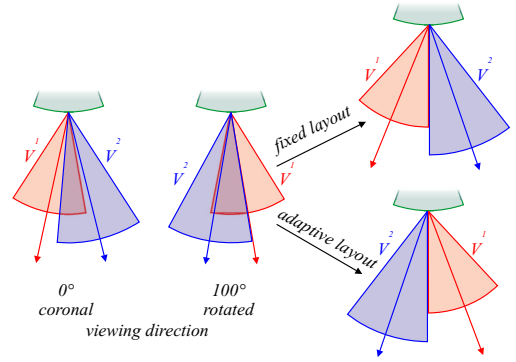


Figure 9: Different layout definition

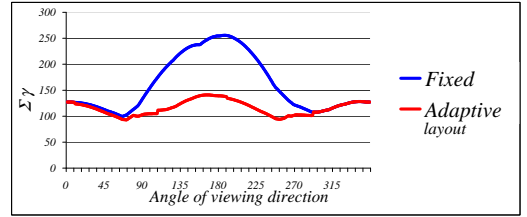


Figure 10: Comparison of introduced distortion.

lines are transformed according to the rotational matrix $\mathfrak{R}_{H_{center}}$ (see Figure 11a). The scan lines represent those parts of the image in which the corresponding re-sampled data from the dataset are rendered into. Because of the applied transformations the scan lines need not be aligned to the pixel rows of the image.

In order to avoid overlapping areas an appropriate start and end-point for each scan line has to be determined. For this reason a special sort of distance map is build up every time an image is rendered. This distance map is defined by the projected center lines of the vessel tree and its scan lines. In contrast to the traditional distance map the distance metric is not defined by an Euclidean distance but by a distance along scan lines. The result of this operation is a fragmented image space where each vessel segment is assigned a maximally image area.

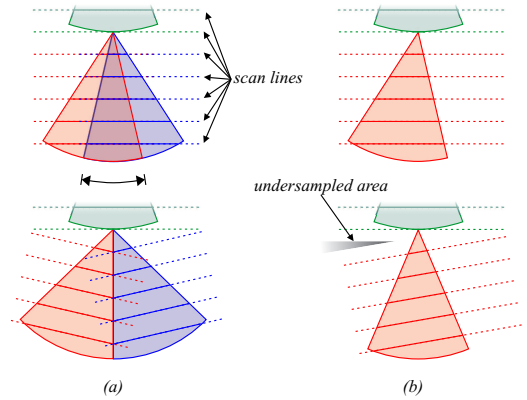


Figure 11: Image space partitioning

4.6 Results

A comparison of stretched multi-path CPR and untangled CPR is presented in Figure 12. In an anterior view the results of the compared methods are rather similar, because there are only few overlapping arteries. In the case of a lateral view the multi-path CPR display provides hardly any diagnostically relevant information. Many superimposed arteries obscure each other. In comparison to that the untangled CPR still provides an unobscured view of the entire vascular tree. Each vessel segment is displayed in diagnostic quality. For instance the stenosis, heavy calcification, and a long occlusion in the left superficial femoral artery is clearly visible. For both untangled CPRs a fixed layout was used.

Figure 13 presents a sequence of untangled CPR images from an abdominal CT-angiographic dataset. A fixed layout was used, and a 1D transferfunction was applied to the re-sampled data approximating the tissue color of the anatomical structures. Areas of arterial wall calcification are shown in the distal abdominal aorta (225°) and in the left internal iliac artery (270°). The abdominal aorta is the main vessel in the upper half of the image. It is branching into the left and right iliac (pelvic) arteries where left and right in the image is interchanged due to the patient orientation. The pelvic artery branches into the thicker external pelvic artery and the thinner inner pelvic artery.

Even though the examination is intended to be done on a small set of pre-computed images, the performance of the algorithm is acceptable for applications in the clinical workflow. The displayed untangled CPR image in Figure 12 was calculated from a real world dataset with a scanned resolution of $512 \times 512 \times 988$ voxel and an original image size of 1164×1097 pixel. The average rendering time per image of the current Java based implementation on a PC workstation with an Intel PIII 1GHz main processor took 2.3 seconds.

5 CONCLUSIONS AND DISCUSSION

Two methods for efficient vessel visualization were proposed. In both methods the spatial coherence of the investigated objects was relaxed to a certain degree.

The helical CPR technique is a new way to display the volume of vascular structures. The motivation for this visualization technique was not an imitation of the natural appearance of the object but the disclosure of diseased vessel segments. Helical CPR visualizes the interior of a vessel in a single image. Re-sampling a spiral around the vessel central axis does not involve any compositing of samples. Therefore no features of the vessel may be hidden by other structures as long as the vessel area is sampled densely enough. This explorative study has shown that the detection of vessel abnormalities is possible from such visualizations which literally peel-off the vessel volume. A particularly attractive future application of this technique is visualization of coronary artery disease from recently developed electrocardiographically gated CT.

The untangled CPR has significant advantages over existing multi-path CPR techniques. This new technique produces an unobscured display of a vascular tree, independent of the viewing direction. Small rotations around the branching points of a vessel tree eliminate occlusions. Therefore the size of the introduced distortion is kept small.

Even though the use of image space is not optimal, the main requirement of unobscured display of vessels from any viewing direction is fulfilled. In addition, untangled CPR preserves isometry which is an important requirement for vascular lesion assessment. The potential for clinical application of this technique is obviously – a more efficient way to assess any complex arterial trees for the presence and extent of vascular disease. Clinical validity and applicability to other vascular territories are currently investigated.

6 ACKNOWLEDGEMENTS

The authors would like to thank Michael Knapp for the generation of the phantom dataset. The work presented in this publication has been funded by the ADAPT project (FFF-804544). ADAPT is supported by *Tiani Medgraph*, Vienna (<http://www.tiani.com>), and the *Forschungsförderungsfonds für die gewerbliche Wirtschaft*, Austria. See <http://www.cg.tuwien.ac.at/research/vis/adapt> for further information on this project.

REFERENCES

- [1] S. Achenbach, W. Moshage, D. Ropers, and K. Bachmann. Curved Multiplanar Reconstructions for the Evaluation of Contrast-Enhanced Electron-Beam CT of the Coronary Arteries. In *Am. J. Roentgenol.*, pages 895–899, 1998.
- [2] Brian Avants and James Williams. An Adaptive Minimal Path Generation Technique for Vessel Tracking in CTA/CE-MRA Volume Images. In *MICCAI 2001*, pages 707–716, 2000.
- [3] P. Felkel, A. Fuhrmann, A. Kanitsar, and R. Wegenkittl. Surface Reconstruction Of The Branching Vessels For Augmented Reality Aided Surgery. In *BIO SIGNAL 2002*, pages 252–254, June 2002.
- [4] Horst Hahn, Bernhard Preim, Dirk Selle, and Heinz-Otto Peitgen. Visualization and Interaction Techniques for the Exploration of Vascular Structures. In *IEEE Visualization 2001*, pages 395–402. ACM, October 2001.
- [5] Sha He, Ruping Dai, Bin Lu, Cheng Cao, Hua Bai, and Baolian Jing. Medial Axis Reformation: A New Visualization Method for CT Angiography. *Academic Radiology*, 8:726–733, 2001.
- [6] Armin Kanitsar, Dominik Fleischmann, Rainer Wegenkittl, Petr Felkel, and Meister Eduard Gröller. CPR - Curved Planar Reformation. In *IEEE Visualization 2002*, pages 37–44. ACM, October 2002.
- [7] Armin Kanitsar, Rainer Wegenkittl, Petr Felkel, Dominik Fleischmann, Dominique Sandner, and Eduard Gröller. Computed Tomography Angiography: A Case Study of Peripheral Vessel Investigation. In *IEEE Visualization 2001*, pages 477–480. ACM, October 2001.
- [8] A. Koechl, A. Kanitsar, F. Lomoschitz, E. Groeller, and D. Fleischmann. Comprehensive assessment of peripheral arteries using multi-path curved planar reformation of CTA datasets. In *Europ. Rad.*, volume 13, pages 268–269, 2003.
- [9] Geoffrey Rubin, Andrew Schmidt, Laura Logan, and Mark Sofilos. Multi-Detector Row CT Angiography of Lower Extremity Arterial Inflow and Runoff: Initial Experience. In *Radiology 2001*, pages 146–158, 2001.
- [10] O. Wink, W. Niessen, and M. Viergever. Fast Delineation and Visualization of Vessels in 3-d Angiographic Images. *IEEE Transactions on Medical Imaging*, 19:337–346, 2000.
- [11] C. Zahlten, H. Juergens, and H. Peitgen. Reconstruction of Branching Blood Vessels from CT-Data. In *Eurographics Workshop on Visualization in Scientific Computing*, pages 161–168, 1994.



Figure 12: A peripheral CTA dataset rendered from coronal and sagittal view using stretched multi-path CPR (a, c) and untangled CPR (b, d) respectively (fixed layout)

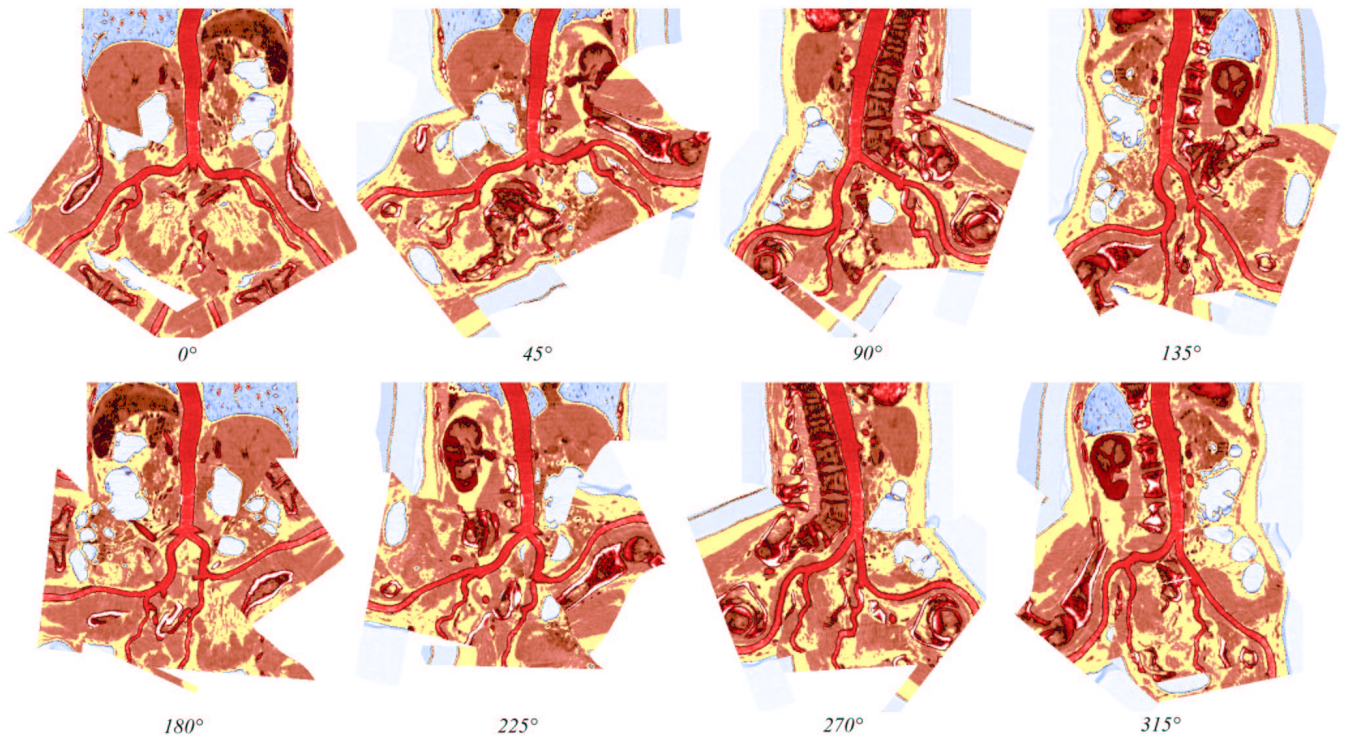


Figure 13: A color coded sequence of untangled CPR images from different re-sampling directions.